Tree Physiology 00, 1–19
doi:10.1093/treephys/tpy097

Invited review

Xylem functioning, dysfunction and repair: a physical perspective and implications for phloem transport

Wilfried Konrad[1,2,6], Gabriel Katul[3], Anita Roth-Nebelsick[4] and Kaare H. Jensen[5]

[1]Department of Geosciences, University of Tübingen, Hoelderlinstrasse 12, D-72074 Tübingen, Germany; [2]Institute of Botany, Technische Universität Dresden, Zellescher Weg 20b, D-01217 Dresden, Germany; [3]Nicholas School of the Environment and Earth Sciences, Levine Science Research Center, Duke University, Durham, NC 27708-0328, USA; [4]Deptartment of Palaeontology, State Museum of Natural History Stuttgart, Rosenstein 1, D-70191 Stuttgart, Germany; [5]Department of Physics, Technical University of Denmark, Fysikvej Building 309, DK-2800 Kgs. Lyngby, Denmark; [6]Corresponding author (wilfried.konrad@uni-tuebingen.de)

Received May 31, 2018; accepted August 8, 2018; handling Editor Teemu Holtta

Xylem and phloem are the two main conveyance systems in plants allowing exchanges of water and carbohydrates between roots and leaves. While each system has been studied in isolation for well over a century, the coupling and coordination between them remains the subject of inquiry and active research and frames the scope of the review here. Using a set of balance equations, hazards of bubble formation and their role in shaping xylem pressure and its corollary impact on phloem pressure and sugar transport are featured. The behavior of an isolated and freely floating air bubble within the xylem is first analyzed so as to introduce key principles such as the Helmholtz free energy and its links to embryonic bubble sizes. These principles are extended by considering bubbles filled with water vapor and air arising from air seeding. Using this framework, key results about stability and hazards of bubbles in contact with xylem walls are discussed. A chemical equilibrium between phloem and xylem systems is then introduced to link xylem and osmotic pressures. The consequences of such a link for sugar concentration needed to sustain efficient phloem transport by osmosis in the loading zone is presented. Catastrophic cases where phloem dysfunction occurs are analyzed in terms of xylem function and its vulnerability to cavitation. A link between operating pressures in the soil system bounded by field capacity and wilting points and maintenance of phloem functioning are discussed as conjectures to be tested in the future.

Keywords: air seeding, cavitation, embryonic bubbles, osmoregulation, plant hydraulics, sucrose transport.

Introduction

Plants are Earth's primary solar energy collectors, and their combined mass exceeds all other life forms on the planet. To achieve this impressive feat, they rely on a range of physio-chemical mechanisms. Among these are long-distance transport of water and assimilates. The focus of this review is characterizing basic biophysical processes that are necessary for long-distance transport in vascular land plants and elucidating some of the fundamental limitations they impose on plant life.

Plants evolved in and were for the longest part of their history restricted to aquatic habitats. In such a habitat, water was ubiquitous and sunlight and carbon dioxide, the other two ingredients of photosynthesis, were consistently available. The adaptation to a terrestrial lifestyle prompted the development of distinct subaerial and aboveground organs. Roots were assigned the extraction of water and (micro-)nutrients from the soil system while the green parts became exclusively responsible for the assimilation of water, carbon dioxide and sunlight into carbohydrates. Clearly, such a spatial differentiation of functions makes transport systems for the distribution of water and carbohydrates within the plant body a necessity. Thus, colonization of land necessitated engineering solutions that resulted in the development of xylem and phloem, the two main conveyance systems in plants. Because the exchange of water and carbohydrates occurs mainly between roots and leaves (i.e., the main suppliers and consumers of water and carbohydrates), it is not surprising

that xylem and phloem functioning are partially coupled. The physical and physiological mechanisms responsible for their functioning and partial coupling frame the compass of the work here and are summarized in Figure 1.

Perhaps the most striking difference between xylem and phloem functioning is that the former is driven by the purely physical mechanisms of transpiration, which functions for some extended time even with dead trees, while the latter requires energy input from living plant cells and water supply from the xylem. In terms of energy demand, xylem water transport is reasonably 'cheap' for the plant as no active pumping is required. The downside is that xylem water is in a thermodynamically metastable state of tension and water transport from the soil to the leaves is prone to hydraulic failure. It may come as a surprise that plants still rely on this mode of water transport in the xylem despite some 400 million years of evolution.

Metastability also complicates even the most delicate experiments as it is often difficult to a priori discern whether an experimental result describes the functioning of the system or its collapse into a stable state, due to disturbances caused by the measurement act. Hence, reliance on theoretical description of the xylem system and its interaction with the phloem must complement measurements so as to push the understanding of the two transport systems as far as possible.

Proceeding in this spirit, the work here first considers the functioning, dysfunction and repair of the xylem water transport system, which is a necessary first step to inquire about phloem transport. The implications of this physical perspective for the partial coupling between xylem and phloem is then evaluated.

Xylem water transport

Plants require a reliable supply of water because (i) water is inevitably lost from plant tissues by transpiration, (ii) water flow distributes dissolved nutrients such as nitrogen, phosphorus or potassium within the plant, (iii) the phloem transport exchanges water with the xylem system and (iv) the process of photosynthesis does require small amounts water as raw material (though this amount is far smaller than transpirational losses).

The problem of water supply became acute when land plants began to grow higher than a few centimeters (leading to a race upwards). Water must be elevated against the gravitational force, which is made more difficult by the increasing conduit lengths that lead to increased frictional losses of energy. To a lesser extent, increasing height above the ground also resulted in the main foliage encountering dryer atmospheric states. Hence, the taller a plant grows, the greater becomes the difference between the atmospheric humidity close to its leaves and the nearly saturated humidity within its leaves. Since this difference is presumed to be a 'driving force' for transpiration (analogous to Dalton's 1802 evaporation law), taller plants transpire more water than short plants, necessitating a more elaborate water transporting system (Raven 1984, 1993, 2003, Raven and Edwards 2004, 2014).

Conducting bundles were present in early land plants with an upright growth habit as indicated by macroscopic remains of plants with cooksonioid (after *Cooksonia*, an extinct group of primitive land plants) or rhyniophytic organization as early as the Late Silurian. These plants consisted of dichotomously branching and leafless axes with *Rhynia gwynne-vaughanii* or *Aglaophyton major* being iconic examples (see Figure 2). However, the water-conducting cells of these early land plants were diverse: *A. major*, for example, did not possess 'genuine' xylem but rather a cell type more similar to moss hydroids. During the Devonian, size and complexity of plants increased rapidly and trees were well established during the Late Devonian, among them *Archaeopteris* as the first tree with secondary xylem similar to that of conifers (Lucas et al. 2013).

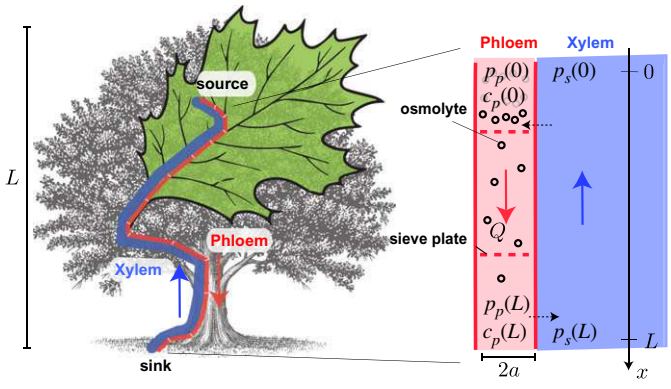

Figure 1. Impact of xylem conditions on phloem transport. Photoassimilate transport in the phloem is powered by differences in osmolyte concentration c_p between source ($x = 0$) and sink ($x = L$), which generates a pressure drop $\Delta p_p = p_p(0) - p_p(L)$ in the phloem. The solute concentration required to maintain constant transport depends on the xylem tension p_s (Eq. (29)).

Short history of the cohesion-tension theory

Modern attempts to understand water transport in plants date back to about 400 years ago when William Harvey (1628) and Marcello Malpighi (1661) drew analogies with blood circulation in animals (Scott 1927). In 1727, Stephen Hales could show (Floto 1999) that water flow in trees is upwards from the soil to the leaves. An important step towards the cohesion-tension theory's development was Heinrich Cotta's identification of sapwood as the transporting plant tissue (Cotta 1806), the result of a prize competition organized by the Imperial Academy of Scientists in Erlangen in the year 1798. The question for the driving force of water movement became the subject of heated debates between 'vitalists' and 'physicists'. The first group contended the idea that living cells should play a major role in the transport mechanism, although they were neither able to identify these cells nor to suggest a detailed transport mechanism.

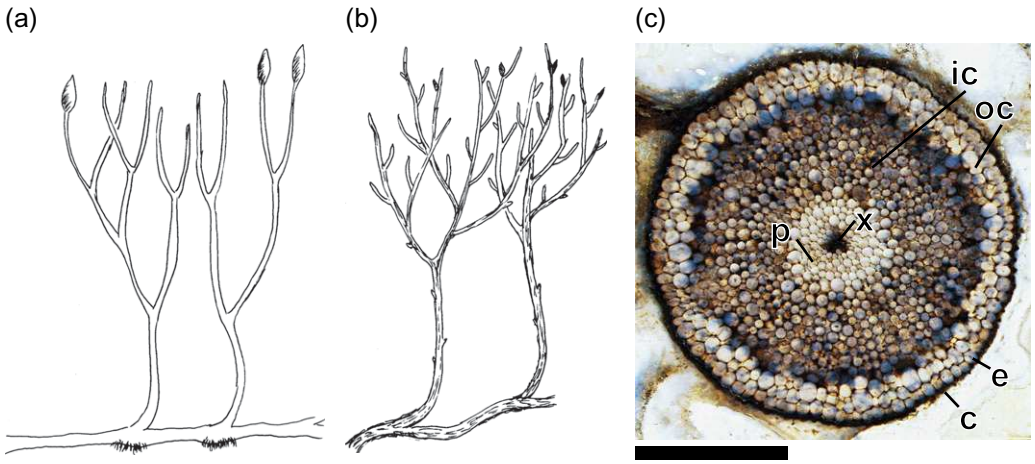

Figure 2. Reconstruction of early land plants (a) *Aglaophyton major* and (b) *Rhynia gwynne-vaughanii* (Lower Devonian, 410 Ma) from the Rhynie cherts near Aberdeen (Scotland). *Rhynia* is one of the earliest known vascular plants. Height: about 20 cm. (c) Transverse section through a *Rhynia* axis showing xylem (x), 'phloem' (p), inner cortex (ic), outer cortex (oc), epidermis (e) and cuticle (c), scale bar = 1 mm. Images (a) and (b) redrawn after (Kenrick and Crane 1997), image (c) by courtesy of the Department of Palaeobotany, University of Münster.

The 'physicists' view that only dead cells are involved, hence, the mechanism of water transport must rely directly on physical effects, was confirmed by an experiment conducted by Eduard Strasburger (1891). Strasburger immersed the roots of a tree into a concentrated solution of copper sulfate ($CuSO_4$). Although the $CuSO_4$ killed all living cells in its way almost instantly, it moved upwards into the leaves (which became evident when they were killed, too). Moreover, the uptake of the solution and the process of transpiration from the dead leaves went on for several weeks afterwards. Shortly after these seminal experiments, Dixon and Joly (1894) showed that water is lifted up against gravity even if the leaves of a detached twig is put into a pressure vessel and kept there under three bars overpressure while the lower end of the twig is put into a water reservoir and kept under atmospheric pressure.

That water can withstand high tensional forces was contradictory to everyday experiences back then, given the inability of water to resist shear stresses. Experiments by Berthelot (1850) and Jäger (1892) showed that water can withstand high tensional forces though some debate followed on whether such experiments actually measured the cohesive forces of water or the adhesive force of water on solid tubes.

The last missing element of the cohesion-tension theory was provided more or less independently by John Joly and Henry Horatio Dixon, both of Trinity College Dublin, and by Eugen Askenasy of Heidelberg University in 1894 (afterwards they quarreled about priority): they found that in the leaf parenchyma where transpiration takes place, a curved water/air interface develops providing the surface tension that counteracts the weight of the water column and pulls it up against gravity (Brown 2013). With Dixon's book from 1914 ('Transpiration and the Ascent of Sap in Plants' (Dixon 1914)) the cohesion-tension theory found its final form. Accounts of historical and recent developments of the cohesion-tension theory can be found in Tyree and Sperry (1989) and Tyree and Zimmermann (2002). For a detailed description see Brown (2013).

Outline of the cohesion-tension theory

Plant water transport in vascular plants relies on two basic principles: (i) transpiration in the leaves provides the driving force that allows water flow to overcome the gravitational pull and frictional forces between water molecules and the vessel, and (ii) the cohesion of water is sufficient to maintain water molecules bound together during the transport phase to leaves.

To illustrate the coordination of these two principles, imagine a long chain (or rather a three-dimensional network) of water molecules whose upper end is fastened to the parenchyma tissue of a plant leaf where transpiration, the transformation of liquid water into water vapor, occurs. From there, the chain hangs down through twigs, trunks, stem and roots into soil water. Each chain link adheres to its neighbors by electromagnetic forces (van-der-Waals forces) that are established due to the highly inhomogeneous and different distributions of positive and negative electric charges within the water molecule (another example of the biological fruitfulness of the physical 'anomaly' of water, as compared with other liquids). Every water molecule that evaporates in the leaves draws up the entire chain for about one molecular diameter. Pushing this analogy further, the higher up in the chain a link (=water molecule) is, the higher the load it has to carry, because the latter consists of the weight of all molecules below. This is why a chain that is hanging down can be expected to break at its uppermost link. Thus, the tension in the water chain increases towards the crown of the tree. When the chain is drawn up by evaporation or loss of water molecules to the atmosphere, friction between the water molecules and the

vessel walls adds to the tensile forces within the water molecules forming the chain.

The following calculation gives an 'order of magnitude' estimate of the stresses acting upon the water in a plant conduit in a hydrostatic state. A water column of cross section A hanging down a distance h exerts a force $G = \rho Ahg$ onto its attachment (with $\rho = 10^3 \mathrm{kg/m^3}$ = density of water, $g \approx 10 \mathrm{m/s^2}$ = gravitational acceleration at the surface of the earth). With trees not exceeding a maximum height ($h_{max} \approx 120 \mathrm{m}$), a lower limit of the magnitude of the stress that the uppermost molecular layers of the water column within the conduit of a tree must be able to resist is given by

$$p_g = \frac{G}{A} = \rho g h \lessapprox \rho g h_{max} = 1.2\,\mathrm{MPa} \quad (1)$$

This estimate is crude because it only accounts for the weight of the water column and neglects additional resistances due to friction. In fact, realistic stresses may be higher by an order of magnitude (see Larcher 2003, Hopkins and Huner 2004, Taiz 2006).

Experimentally, it is difficult to distinguish resistance against shear stress from resistance against tension stress because it is not easy to apply only one of the two stress varieties to liquid water. Hence, measurements of the breaking strength of water against tension stress may be more informative about the quality of the experimental setup than reporting the true value of breaking strength of water. Nonetheless, such experiments can provide a reliable lower limit. From the literature, values of the breaking strength of water range between 50 MPa and 100 MPa and this range seems to be (i) reliable and (ii) in accordance with theoretical considerations (Temperley and Trevena 1994). Hence, even if realistic stresses are much higher than the 1.2 MPa estimated above for the water in a tree conduit, they appear well below the lower limit of the breaking strength of water.

Inside a tree, juxtaposition of this physical limit of breaking strength of water may be an overestimate. Values of breaking strength have been measured or derived for pure water that contains insignificant quantities of molecular species other than water (for example no air bubbles). The reason for this restriction is found in the radial characteristics of the intermolecular force between water molecules: for distances smaller than an equilibrium separation r_{eq}, two water molecules exchange a repulsive force (whose large strength accounts for the small compressibility of water). For separations greater than r_{eq}, the molecules attract each other. The attractive force has a maximum at a separation r_{max}. If the separation is increased further, the attraction decreases and becomes eventually effectively zero.

When water is contaminated by other molecular species, some water molecules become farther separated from one another than they were before (in pure water) because molecules of the contaminating species have entered the space between them. If this effect shifts the mean separation between adjacent water molecules to values much beyond r_{max}, the attractive force between these water molecules decreases. It directly follows that the effective breaking strength of the whole network of water molecules (or the chain) is reduced. If the breaking strength is reduced far enough, this effect becomes catastrophic. It should be noted, however, that solitary molecules that are completely surrounded by water molecules (macroscopically speaking, they are dissolved in water) do not usually represent a threat to the integrity of the network of water molecules. Soil particles or air bubbles, however, may become dangerous if their diameter is large enough. To minimize this threat, the roots of (vascular) plants have developed excellent filter systems able to keep these contaminants out of the flow path (see, e.g., Sitte et al. 2002).

Interrelation with phloem transport

Photosynthesis in plant leaves converts light into chemical energy that is stored in sugar molecules for later use in metabolism, growth and reproduction. Sugars are exported from the leaf by bulk liquid flow under positive pressure through phloem sieve elements, which form a microfluidic tube network linking distal parts of the plant (Stroock et al. 2014). The flow is driven by osmotic pressure differences between sugar sources in leaves and sinks at sites where sugars are consumed, as shown in Figure 1. Phloem sap contains a plethora of osmolytes, but the primary determinant of phloem pressure is the concentration of sugars and small ions (Jensen 2018). Phloem transport thus relies on the osmotic exchange of water with the xylem system, and the conditions in the xylem have a direct impact on phloem flow (Sevanto 2018).

Briefly, when incident photosynthetic photon flux density is >0, photosynthesis commences in leaves, the byproduct of which are sugars. Assimilated sugars that accumulate in the mesophyll are transported to companion cells and subsequently to sieve elements in the so-called loading zone (i.e., leaf). The loading is achieved by molecular diffusion (i.e., passive and common in angiosperm and gymnosperm) or polymer trapping and apoplastic pumping (i.e., active and common in herbaceous species) mechanisms (Jensen et al. 2016). The production rate of sucrose in the loading zone can be approximated by $\alpha_p(\beta f_c A_l)$, where f_c is the photosynthetic rate that is linked to the transpirational losses from leaves (quantified by a water-use efficiency), $\alpha_p (\in [0,1])$ and β are species-specific loading efficiency and the number of sucrose molecules produced from one assimilated CO_2 molecule ($\beta = 1/12$ for sucrose only), respectively. The $\alpha_p = 1$ when all sucrose molecules produced from f_c enter the loading zone.

The total water potential in the phloem loading zone includes turgor pressure (p_p), the aforementioned hydrostatic pressure p_g given by Eq. (1) and the osmotic potential (Π) that increases with increasing sugar concentration (due to f_c) and is presumed

to be the dominant term. If chemical and thermal equilibrium exist between the phloem and xylem shown in Figure 1, then $p_s + p_g \approx p_p + p_g - \Pi$, where p_s is the xylem pressure in the most distal part (i.e., vicinity of the leaf) assuming negligible sugar concentration in the xylem. The p_s is impacted by all the hazards associated with formation of air bubbles in the xylem arising from the metastable state of water whereas Π is dictated by sugar accumulation arising from finite f_c. This review is primarily focused on the hazard of bubble formation and their role in shaping p_s as well as their subsequent impact on Π.

Hazards to water transport

Basics and preliminaries

As noted earlier, one of the main hazards to water transport is its metastable state, which is prone to bubble formation and subsequent embolism. In fact, Haberlandt already noted (in 1914) that 'Vessels and tracheids normally contain both, air and water, the relative amounts of the two substances vary according to the season and the time of day'. There is now recognition that formation of gas emboli are common occurrences in the xylem of many plant species. This section reviews basic concepts on bubble stability within a xylem vessel. A gas bubble immersed in a xylem fluid and filled with air and water vapor may experience the following balance situations:

(i) A balance of mechanical forces: (a) the randomly moving gas molecules inside the bubble act as an outward directed force that tries to expand the bubble; (b) the surface tension of the gas/liquid interface tries to contract the bubble; (c) the pressure p_s of the xylem water contributes to the expanding force for $p_s < 0$ and to the contracting force for $p_s > 0$.

(ii) A balance with respect to the exchange of water molecules with the bubble's surroundings: if the water vapor partial pressure within the bubble differs from the water vapor saturation pressure, water molecules either condensate at the bubble's gas/liquid interface or vaporize from there into the bubble.

(iii) A balance with respect to the exchange of air molecules with the bubble's surroundings: the number of air molecules remains constant only if a 'diffusional equilibrium' prevails between the air partial pressure within the bubble and the concentration of air molecules dissolved in the xylem water. Otherwise, air molecules from within the bubble either dissolve at the bubble's gas/liquid interface in the xylem water and diffuse towards regions of lower air molecule concentration, or else a diffusional current through the xylem water delivers air molecules to the bubble surface and into the bubble.

Since the exchange process between water vapor and water is faster than the exchange of air by a factor of about 10^6 and since the dissolution of a bubble filled merely with water vapor of an initial radius of 1 μm immersed in water with $p_s = -1$ MPa lasts about 2.9×10^{-10} s, in what follows it is assumed that bubbles are balanced with respect to the first two situations but not necessarily with respect to the third. Depending on whether a bubble consists merely of water vapor or contains additionally air molecules, two effects that are potentially hazardous for the conductance of the xylem vessels and the xylem potential must be considered:

- spontaneous cavitation
- air seeding.

Spontaneous cavitation

Spontaneous cavitation arises due to statistical fluctuations (caused, for instance, by Brownian movement) of the energy of a group of neighboring water molecules in liquid state. If these molecules acquire enough kinetic energy to 'cut' the network of intermolecular binding forces defining the liquid state and to become a cluster of gaseous molecules, then an embryonic bubble filled with water vapor forms within the liquid. Whether this embryonic bubble disappears soon afterwards because its constituents are being 'resorbed' into the liquid surrounding the bubble or whether it grows because more water molecules vaporize into it depends (i) on its initial radius R_0 and (ii) on the tension $p_s < 0$ (=negative water pressure) existing in the water column.

The reversible free energy (referred to as the Helmholtz free energy in thermodynamics) associated with the spontaneous formation of an embryonic bubble with radius R is given by (see Debenedetti 1996, Oertli 1971, Pickard 1981)

$$W(R) = 4\pi\gamma R^2 - \frac{4\pi}{3}(p_w - p_s)R^3 \qquad (2)$$

(γ: surface tension of air/water interface, p_w: pressure of water vapor within the bubble, p_s: water pressure) and depicted in Figure 3a.

The further development of the gas bubble is essentially controlled by forces obtained from Eq. (2) by differentiation:

$$\partial W/\partial R = 8\pi\gamma R - 4\pi p_w R^2 + 4\pi p_s R^2 \qquad (3)$$

- The first term on the right-hand side represents the contracting surface force exerted by the liquid/gas-interface at the bubble surface.
- The second term represents the expanding gas pressure of water vapor and air molecules.
- The third term represents the xylem water pressure; for $p_s > 0$ it has a contracting effect on the gas bubble, for $p_s < 0$ an expanding effect.

A bubble of radius R that neither expands nor contracts because the respective forces are at equilibrium is characterized

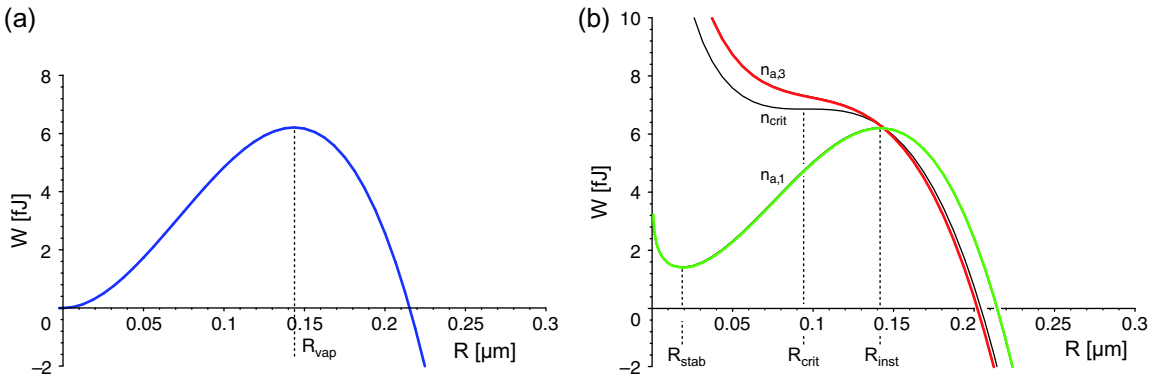

Figure 3. Energy of bubble formation $W(R)$ plotted against bubble radius R. For illustration, water pressure in the conduit is set to $p_s = -1$ MPa. Equilibrium between expanding and contracting forces is realized only at bubble radii R representing extrema of $W(R)$. Maxima indicate unstable, minima stable equilibrium. (a) Bubble filled only with water vapor. (b) Bubble filled with water vapor and air. Curves are plotted for the following numbers of air molecules: $n_{a,1} = 7.5 \times 10^{-20}$ mol, $n_{crit} = 7.5 \times 10^{-19}$ mol and $n_{a,3} = 9 \times 10^{-19}$ mol.

by $\partial W/\partial R = 0$. In molecular terms, the number of water vapor molecules vaporizing into the bubble equals the number of molecules condensing into the surrounding liquid at equilibrium. In the case $\partial W/\partial R > 0$, condensation dominates and the bubble disappears. For $\partial W/\partial R < 0$, vaporization is the dominating effect and the bubble expands further. To locate the extrema of $W(R)$ given in Eq. (2), the radius R satisfying $\partial W/\partial R = 0$ must be determined and it must be checked that $W(R)$ is a maximum, not minimum. The solutions for $\partial W/\partial R = 0$ are $R = 0$ (representing an artifact) and

$$R = \frac{2\gamma}{p_w - p_s} =: R_{vap} \qquad (4)$$

The second derivative of $W(R)$, evaluated at R_{vap}, amounts to

$$\partial^2 W/\partial R^2 = 8\pi\gamma - 8\pi(p_w - p_s)R|_{R=R_{vap}} = -8\pi\gamma < 0 \qquad (5)$$

Hence, $R = R_{vap}$ represents a maximum of $W(R)$ corresponding to an unstable equilibrium of forces (whereas a positive value would indicate a minimum of $W(R)$ and a stable equilibrium as may occur when setting $R = 0$). In other words, if the radius R of a spontaneously emerging vapor bubble obeys the relation $R > R_{vap}$, the bubble is unstable and expands (in principle indefinitely). For $R < R_{vap}$, the bubble vanishes (to a stable $R = 0$).

Hence, the stability of an embryonic bubble depends on the value of R_{vap} at its inception. In turn, R_{vap} depends on the reciprocal of the water pressure (or, rather, tension) p_s in the bulk xylem. Thus, the more negative the water pressure is, the smaller is the bubble radius dividing the regimes of bubble collapse and expansion. For example, under a water pressure of $p_s = -0.01$ MPa, all bubbles with a radius smaller than $R_{vap} \approx 10.94\,\mu$m will collapse immediately. For the more negative pressure $p_s = -1$ MPa this radius amounts to the much smaller value $R_{vap} \approx 0.143\,\mu$m (see Figure 3 and the discussion in Oertli 1971). Put differently, a bubble of initial radius $R \approx 5\,\mu$m collapses (without doing harm to the xylem system) under a water pressure of $p_s = -0.01$ MPa but expands until embolism under $p_s = -1$ MPa. The actual bubble growth phase requires consideration of other factors such viscous forces, inertia and unsteadiness that are represented by the so-called Rayleigh–Plesset equation (briefly considered later on).

Irrespective of the details of bubble growth, this analysis suggests that a water column under tension constitutes a metastable system in the following sense: if the water column is 'disturbed' by the introduction of an embryonic bubble of radius $R < R_{vap}$, then the bubble dissolves. For $R > R_{vap}$, however, the bubble inflates until the water column collapses into a stable state characterized by a positive water pressure $p_s > 0$.

Based on arguments from statistical physics and thermodynamics, it has been shown (Maris and Balibar 2000, Oertli 1971, Pickard 1981) that for the negative pressures to be expected in plant conduits spontaneous cavitation plays only a minor role in causing embolism (as compared with the air seeding process, see below) because the tension values occurring in the xylem are not high enough to permit a significant formation rate of expanding bubbles. Oertli (1971) calculates that in a xylem system consisting of 1 litre = 10^{-3} m^3 water and being under a pressure $p_s = -127$ MPa an embolism occurs (on average) every 100 years. If p_s increases only slightly (meaning a decrease in $|p_s|$) the time span without embolism increases tremendously. Put differently, the probability of a spontaneous bubble formation is for $p_s > -100$ MPa (meaning $|p_s| < 100$ MPa) essentially zero. Trees function far away from this value.

Air seeding

Air seeding can occur when a group of 'air' molecules find their way into a water conduit. Since a completely impermeable material does not exist in biological (nor in artificial) tissues, tiny leaks will always and everywhere be present. Larger cracks and openings in wood may be produced by the wind bending twigs

of the tree as a whole, or by animals such as woodpeckers or beetles in search of food.

To describe this mixture of water vapor and air, Eq. (2) is now extended by introducing a term representing the n_a air molecules (Shen et al. 2002, 2003) resulting in (cf. Figure 3b)

$$W(R) = -\frac{4\pi}{3}(p_w - p_s)R^3 + 4\pi\gamma R^2 + 3\mathcal{R}Tn_a \log\left(\frac{R_{max}}{R}\right) \quad (6)$$

where $\mathcal{R}$ is the gas constant, and two arbitrary constants have been chosen such that (i) in the absence of air molecules (i.e., $n_a = 0$, that is, in the case of a water vapor bubble) the formation energy W vanishes for $R = 0$, and (ii) the contribution of the air molecules to the formation energy $W(R)$ (the last term in Eq. (6)) vanishes for $R = R_{max}$.

$$R_{max} := \frac{2\gamma}{-p_s} \quad (7)$$

denotes the maximum equilibrium radius that a gas bubble immersed in water of negative pressure $p_s < 0$ can attain (see Konrad and Roth-Nebelsick 2003; a rigorous derivation of Eq. (6) can be found in Debenedetti (1996)).

The analysis of the compressing and expanding forces acting upon a bubble will be based upon Eq. (6). For these calculations, the following two assumptions are made:

- $p_w \approx p_w^{sat}$ (p_w^{sat}: saturation vapor pressure that only varies with temperature). The exchange of water molecules between a bubble and surrounding liquid is a very intensive one (for a quantitative estimate of the exchange intensity see Adamson and Gast (1997)). Therefore, the water vapor partial pressure in the bubble readjusts to the water vapor saturation pressure almost immediately.
- $n_a \approx$ const.: this assumption is only valid on very short time scales associated with bubble formation considered here. The following observations corroborate its plausibility: (i) the low solubility of air in water, implying that only a small fraction of the air molecules in the bubble's interior are lost to the surrounding liquid within the considered time scale, and, (ii) the slowness of diffusional transport in liquids: a rough estimate — employing the relation (traveltime) $\approx$ (distance)$^2/D_{air}$ (where $D_{air} \approx 2.1 \times 10^{-9}$m^2/s) — shows that dissolved air molecules diffusing away from a bubble need about half a day to cover a distance of 1 cm.

Proceeding similarly as above, the bubble radii where equilibrium of forces prevails are found from

$$\partial W/\partial R = 8\pi\gamma R - \left\{4\pi(p_w - p_s)R^2 + \frac{3\mathcal{R}Tn_a}{R}\right\} = 0 \quad (8)$$

and their stability is assessed by evaluating the sign of $\partial^2 W/\partial R^2$ at the equilibrium point(s). Equation (8) represents a cubic equation with respect to R. Its structure suggests that it has one, two or no real and positive solutions depending on the values of the quantities γ, n_a, p_s and p_w. The crucial quantity to be explored here is n_a, the number of air molecules in the bubble, and its relation to

$$n_{crit} := \frac{128\pi\gamma^3}{81\mathcal{R}T}\frac{1}{(p_w - p_s)^2} \quad (9)$$

the maximum number of air molecules that a bubble can accommodate. For $n_a > n_{crit}$, no solutions exist. For $n_a = n_{crit}$ one solution exists, and for $0 \le n_a < n_{crit}$ two solutions of $\partial W/\partial R = 0$ exist. These two solutions are located at the radii

$$R_{stab} = \frac{R_{vap}}{3}\left(1 - 2\cos\left[\frac{1}{3}\arccos\left(1 - \frac{2n_a}{n_{crit}}\right) + \frac{\pi}{3}\right]\right)$$
$$R_{inst} = \frac{R_{vap}}{3}\left(1 + 2\cos\left[\frac{1}{3}\arccos\left(1 - \frac{2n_a}{n_{crit}}\right)\right]\right) \quad (10)$$

where $R_{vap} = 2\gamma/(p_w - p_s)$.

Air–water vapor bubbles show a more complex behavior than pure water vapor bubbles because their behavior depends on the number n_a of air molecules in the bubble (i.e., a new control variable in the stability analysis):

- Evaluating $\partial^2 W/\partial R^2$, the bubble at radius R_{stab} is in stable equilibrium whereas at radius R_{inst}, it is in an unstable equilibrium (meaning it will show a tendency to expand).
- Eqs (10) imply $R_{stab} \le R_{inst}$. The equality is realized for $n_a = n_{crit}$ when both R_{stab} and R_{inst} (the two equilibrium solutions collide) approach the quantity

$$R_{crit} := \frac{4\gamma}{3(p_w - p_s)} = \frac{2}{3}R_{vap} \quad (11)$$

- For $n_a \to 0$ we find $R_{stab} \to 0$ and $R_{inst} \to R_{vap}$.
- For $n_a > n_{crit}$ both R_{stab} and R_{inst} become undefined, meaning that the bubble expands without limits (see Figures 3b and 4).

The bubble behavior is now illustrated by Figure 3b. A bubble that contains $n_{a,3} > n_{crit}$ air molecules fulfills the condition $\partial W/\partial R < 0$ for all $R > 0$. Equation (8) implies then that the bubble can only expand. If the bubble contains $n_{a,1} < n_{crit}$ air molecules, its future depends also on its initial radius R: in the case $R > R_{inst}$ it expands, in the case $0 < R < R_{inst}$ the bubble expands or contracts towards R_{stab}. Table 1 gives a few values for R_{crit} and n_{crit}.

Figure 4, derived from Eq. (8), illustrates the interdependence of initial radius and air content in a stability diagram formed by the (n_a, R)-plane (the two control variables). It reveals several aspects of embolism potential of an embryonic bubble:

- The ability of an air–water vapor bubble to seed embolism increases with its air content (with the water vapor pressure being constant and only dependent on temperature) (see Figure 4): a bubble of initial radius R_2 containing n_1 air

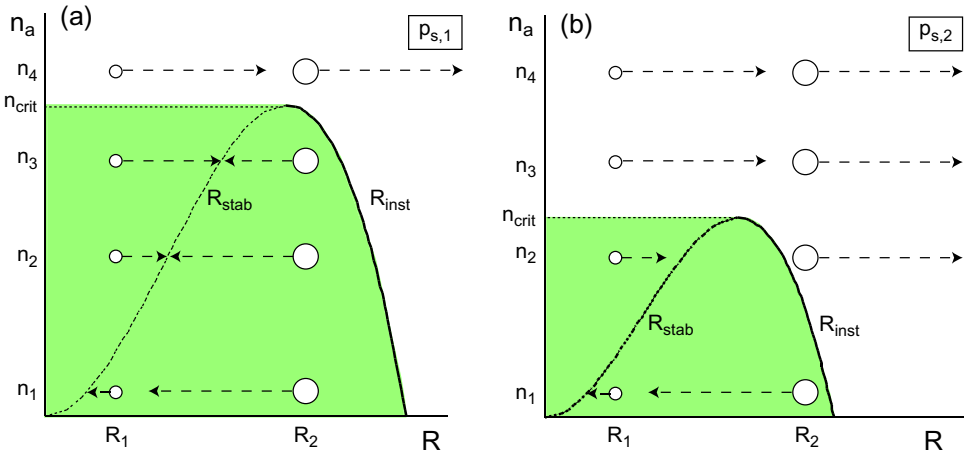

Figure 4. Regions of stability and instability of bubbles of radius R, filled with water vapor and n_a air molecules (cf. Eq. (8)). (a) Stability diagram for a given water pressure $p_{s,1}$. (b) Stability diagram for a water pressure $p_{s,2}$ with $p_{s,2} < p_{s,1}$ (i.e., $p_{s,2}$ is more negative than $p_{s,1}$). Only bubbles lying on the curves R_{stab} (broken line) and R_{inst} (solid line) are in stable or unstable equilibrium. Bubbles represented by other (n_a, R)-values either contract or expand (indicated by broken arrows). Bubbles in the green regions (left and below the solid curves R_{inst}) are contracting or expanding towards the stable radii R_{stab} lying on the dotted curves. Bubbles characterized by (n_a, R)-values outside the stability regions expand. If p_s decreases, the region of stability shrinks. Hence, bubbles that are in equilibrium under water pressure $p_{s,1}$ (such as those inhabited by n_3 air molecules in part (a) of the figure) fall outside of the equilibrium region if p_s drops to $p_{s,2} < p_{s,1}$ (see part (b) of the figure).

Table 1. Values of R_{crit} and n_{crit} calculated from Eqs (9) and (11) for the conduit water pressures p_s given in the first row.

p_s	−1 MPa	-10^{-1} MPa	-10^{-2} MPa
R_{crit}	0.096 µm	0.93 µm	7.29 µm
n_{crit}	7.4×10^{-19} mol	7.0×10^{-17} mol	4.3×10^{-15} mol

molecules contracts towards the stable radius R_{stab}, a bubble of the same initial radius containing n_4 air molecules (with $n_4 > n_1$), however, bursts.

- Because of $p_w \ll |p_s|$ (the water vapor pressure p_w is usually much smaller than the absolute value of the water pressure p_s) the quantities n_{crit}, R_{inst}, R_{stab} and R_{vap} are approximately proportional to the reciprocal of p_s (see Eqs (9), (10) and (4)). Thus, if p_s decreases (i.e., becomes more negative), the stability region that represents all bubbles (of radius R and containing n_a air molecules) drifting to stable equilibrium shrinks. (In Figure 4 the stability regions are the green areas left and below the solid curves R_{inst}.) Hence, bubbles that were within the stability region at a given water pressure may become unstable because the borderline between stability and instability has wandered across their (fixed) location in the (n_a, R)-plane, due to the drop in p_s.
- Immediate collapse of an air–water vapor bubble is impossible. Unlike water vapor molecules, air molecules cannot instantly condense to the liquid state (at least not under temperatures and pressures compatible with living plants). Hence, a stable air–water vapor bubble can only disappear by dissolution through diffusion of air molecules from the bubble into the surrounding water. Whether or not this diffusion will occur depends on the concentration of air molecules already dissolved in the surrounding water. This dissolution and its associated dynamics will be discussed in section 'Diffusional equilibrium and dissolution of floating bubbles'.

Conclusion: spontaneous cavitation vs air seeding

The appearance of an embryonic bubble does not necessarily lead to vessel embolism. For the xylem sap pressures typical for trees, the emergence of bubbles containing only water vapor is extremely unlikely, as discussed in section 'Spontaneous cavitation'. Bubbles containing water vapor and air molecules dissolve, according to section 'Diffusional equilibrium and dissolution of floating bubbles' quite rapidly, provided the bubbles are small enough and do not contain too many air particles. In sufficiently big bubbles, however, the expansion tendency of the gas particles inevitably outweighs the surface tension and the bubble will either grow and fill the vessel or split up into daughter bubbles, which may or may not dissolve. A detailed and explicitly time-dependent exposition of these processes can be found in Konrad and Roth-Nebelsick (2003).

Safety measures against embolism

Experimental evidence of embolism

Cavitation and embolism can be demonstrated indirectly or by direct observation using imaging techniques. Indirect measurement of embolism is mostly conducted by producing vulnerability curves (VC) that express the loss of hydraulic conductivity of a stem or a stem segment against xylem pressure. Different techniques are

applied: air dehydration ('natural' drying of a sample or a whole potted plant), air injection (application of positive gas pressure to the sample, which should provide the same amount of embolism as the corresponding negative pressure) and centrifugation (xylem tension generated by spinning of the stem segment in a centrifuge) (Venturas et al. 2017). Conductivity is mainly measured by driving water through a sample with a defined pressure gradient. Also, xylem tension is difficult to measure because it is in a metastable state sensitive against any disturbance. The most 'practical' way to measure xylem tension is by using the pressure chamber. Here, the sample is exposed to an increasing positive pressure that is monitored with one end of the sample sticking out of the device. Tension is then determined as being identical with respect to the absolute value to that positive pressure necessary to drive liquid to the surface of the cut end (Vogt 2001). Another method is the pressure probe that records the tension directly. Here, a fine capillary is brought into a conduit and the 'pull' of the xylem tension is recorded (Wei et al. 1999). This method is, however, also invasive and can disturb the metastable state of xylem tension.

Although numerous and often consistent results were collected over the years based on these methods, there are still methodological debates (Cochard et al. 2013, Rockwell et al. 2014, Venturas et al. 2017). Various artifacts and problems may occur, particularly with invasive techniques, as may be expected when measuring water in a metastable state. Methods that are based on cutting samples potentially allow bubbles (and other impurities) to enter the sample or water oversaturated with air is pressed into the xylem, which can bias the results (Wheeler et al. 2013, Wang et al. 2014). A critical discussion of invasive approaches has been provided by Cochard et al. (2013).

A non-invasive method is stem psychrometry (Vogt 2001), but attaching the brittle sensors firmly to functional xylem and isolating the contact zone from external influences is quite challenging. Another non-invasive technique is to record acoustic emissions emitted during the cavitation event, which has its own pitfalls (Vergeynst et al. 2014). Direct observation of cavitation and embolism is possible with new imaging techniques such as high-resolution magnetic resonance imaging (Holbrook et al. 2001, Clearwater and Clark 2003) or high-resolution X-ray tomography (synchrotron- or desktop-based) (Brodersen et al. 2010, Cochard et al. 2015, Ryu et al. 2016) and neutron radiography (Tötzke et al. 2013). Another new tool was recently introduced by Brodribb et al. (2017) based on light transmission.

The various experimental problems are accentuating the debate on xylem refilling. Refilling must represent a repair mechanism of dysfunctional conduits thereby recovering hydraulic conductivity. The original concept was that positive pressure was necessary for xylem refilling due to, for example, thorough re-wetting of the soil by extensive rain (Vogt 2001) or root pressure during spring (Sperry et al. 1987). Some years ago, evidence appeared for a 'novel' type of refilling with conduit repair occurring under xylem tension (Salleo et al. 1996, Hacke and Sperry 2003, Stiller et al. 2005). These findings appeared to contradict conventional models on xylem functioning and prompted discussions on the possible mechanisms (Holbrook and Zwieniecki 1999, Tyree et al. 1999, Konrad and Roth-Nebelsick 2003, Vesala et al. 2003). Basically, living cells and particularly the phloem are suggested to be involved (Salleo et al. 1996, Nardini et al. 2011).

The feasibility of this refilling model depends largely on the question of whether the dissolution of the 'embolizing' lumen bubbles can be completed before the hydraulic isolation of the embolized vessel fails due to the dissolution of the pit bubbles. Therefore, the temporal behavior of both spherically symmetric lumen bubble and of axially symmetric pit bubble is of central significance to embolism repair and to the general dynamics of bubbles in xylem conduits. The dynamics of spherically symmetric bubbles and the temporal development of bubbles in cone-shaped pits has been explored in Konrad and Roth-Nebelsick (2003).

By no means is this debate settled and the aforementioned refilling and/or the degree to which conduits can be refilled under negative tension (Venturas et al. 2017) remain open questions. Possible experimental artifacts biasing determinations of xylem tension and embolism/repair continue to emerge. For instance, recent experiments on *Laurus nobilis*, a 'classic' species for which the novel refilling was demonstrated early, provided inconsistent results (Cochard et al. 2015, Nardini et al. 2017). However, deactivating or interrupting the phloem by, for example, girdling, can obviously block refilling, an indication that metabolic processes of living cells are involved in xylem repair (Salleo et al. 1996, Trifilò et al. 2014). New imaging techniques as described above allow for directly observing refilling of conduits. For *Vitis vinifera*, it was indeed shown that the water entering empty conduits occurs through vessel-parenchyma pits and therefore must originate from adjacent living cells (Brodersen et al. 2018). High-resolution observations of refilling conduits indicate a long lifetime of small bubbles seated within the pit region. Moreover, the bubbles persisting during xylem refilling appear to be above the critical radius with respect to the measured xylem tension. Hence, these bubbles should have expanded thereby preventing conduit refill. A possible explanation is that the xylem of *V. vinifera* is segmented and that different xylem pressure values can exist at different xylem locations (i.e., non-uniform pressure distribution). These current controversies and unexpected results demonstrate that despite the availability of new experimental techniques, the process of embolism and embolism repair is not fully resolved.

The most reliable way to circumvent the problems and precariousness that trouble attempts to obtain VCs experimentally is — probably — to refine the theoretical model of conduit embolism to such a degree that it can be used to derive VCs indirectly from experiments based upon 'stable' and unambiguously measurably parameters, defined in the framework of the soil–plant–atmosphere continuum.

Safety measures provided by conduit architecture

Various anatomical features of the xylem can be understood as improving safety against embolism. Their purpose is (i) to avoid embolism altogether, (ii) to minimize its consequences by isolating embolised conduit segments of the water transport pathway and (iii) to reestablish conduit functionality.

There are two types of conduits: tracheids and vessels. Whereas tracheids are elongated single cells, vessels are formed by series of cells whose end walls are perforated or even removed. The latter conduit type can be long, particularly in ring-porous species. However, all conduit types are shorter than the entire transport pathway, and water has to cross from conduit to conduit on its ascent (Figure 5). The transport pathway is therefore segmented, and this segmentation and the structure of the interconnecting pits are essential for transport safety. The role of pits is to allow water to enter and leave conduits and to isolate a cavitated conduit. There are two kinds of pits that are permeable for water but not for gas after a cavitation has occurred.

When an embryonic bubble with $R > R_{crit}$ and/or $n > n_{crit}$ expands within a conduit, the mean distances between the (liquid) water molecules decrease, the water pressure increases. Hence, water molecules are pushed through the pit openings into adjacent conduit elements that are still intact and are under (negative) 'operating pressure'. The two pit types achieve hydraulic isolation of the dysfunctional conduit segment in different ways:

- If a torus-margo pit operates in 'normal mode' the flow velocity is rather low (gymnosperms have maximum flow velocities of 1 m h^{-1} to 2 m h^{-1}), see Larcher (2003) and the flow rate Q through a pit opening (see Figure 6d–f) attains moderate values below a certain critical flow rate Q_{crit}. The two forces acting on the torus — one originates from the flowing water pushing the (impermeable) torus, the other one is exerted by the elastic (and permeable) margo — are in stable equilibrium (see Chapman et al. (1977)) and the torus occupies a somewhat deflected (depending on the flow rate Q) but stable position within the pit.

  In 'embolism mode', the water rushes much more quickly through the pit opening; Q exceeds Q_{crit}, equilibrium between the two forces becomes impossible (see Chapman et al. (1977)) and a stable position for the torus does not exist any more. The torus is pushed against the pit border, the pit closes and remains closed due to the water pressure difference between dysfunctional and intact conduit element (Figure 6f).

- Membrane pits (see Figure 6a–c) possess membranes with numerous tiny pores (typically with a radius of $r_p \approx 0.005\,\mu m$ to 0.02 μm) through which the conduit water flows in 'normal mode' (see Choat et al. (2003)). During embolism, the embryonic gas bubble inflates — perhaps also releasing daughter bubbles — until it touches eventually the pit membrane. In the membrane, pores develop strongly curved gas/water interfaces ('menisci') whose radii of curvature have probably similar values as the membrane pore radii. Hence, according to the Young–Laplace-Equation, the menisci can be expected to withstand pressure differences (related to the r_p values just given) of about

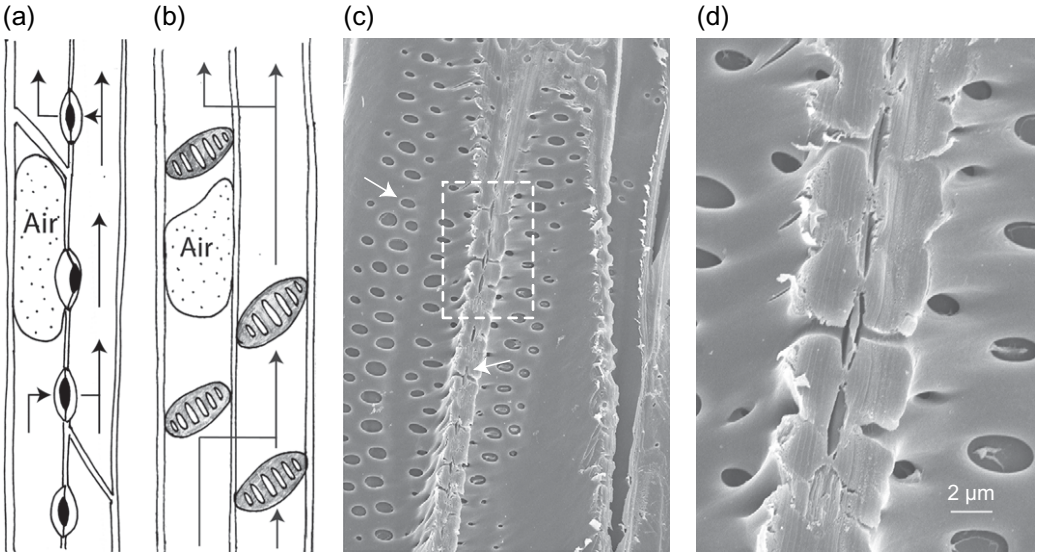

Figure 5. (a) Re-routing of water flow in a conduit with torus-margo pits (typical for gymnosperms) and with (b) membrane pits (typical for angiosperms). In torus-margo pits, a pressure difference in adjacent conduits caused by embolism pushes the torus against the pit opening, the pit closes. Membrane pits possess membranes with tiny openings. In case of embolism, highly curved gas/water interfaces develop in these openings, effectively closing the pit. (c) Adjacent conduits of *Laurus nobilis*. The conduits are cut open along their longitudinal axes. The pits can be seen in cross section (right arrow) and top view (left arrow). (d) Detail of (c). Illustrations (a) and (b) redrawn from Taiz (2006).

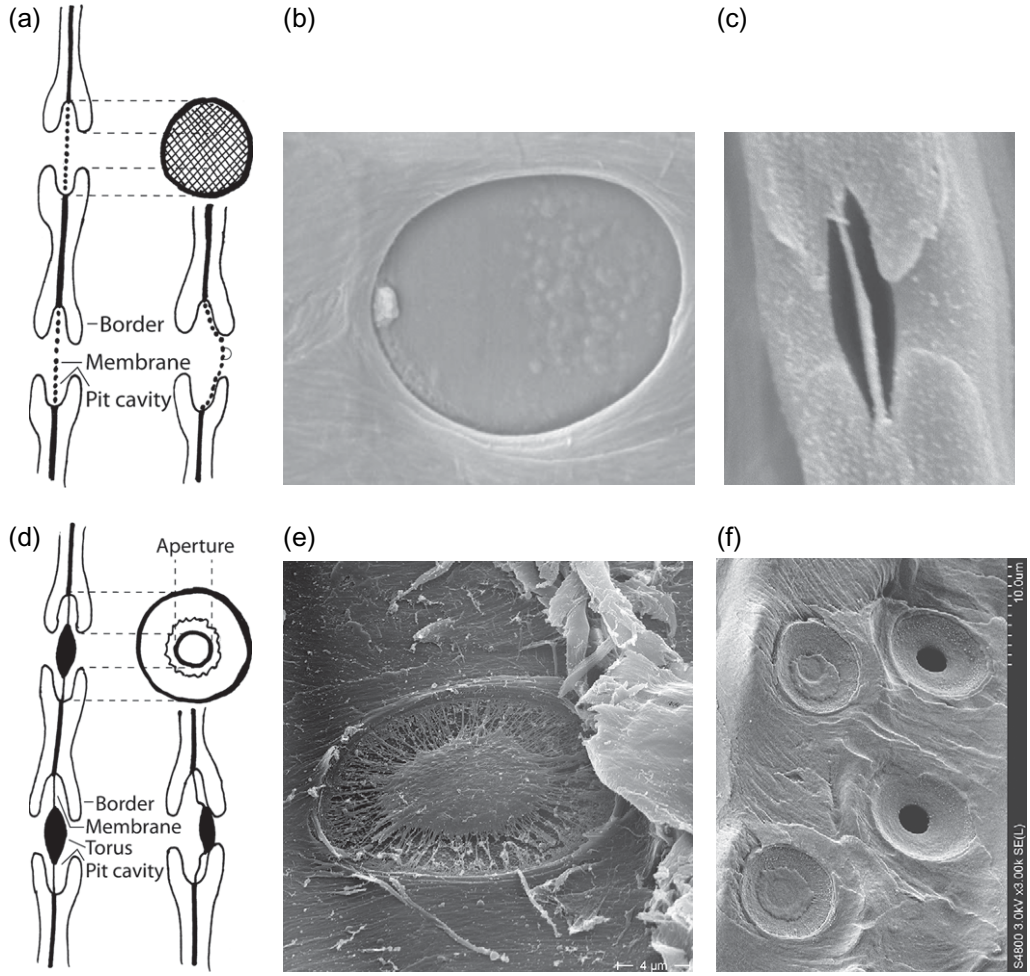

Figure 6. Differences and similarities between membrane pits (a–c) and torus-margo pits (d–f). The membranes in membrane pits possess many tiny pores through which the xylem water flows. During embolism, strongly curved gas/water interfaces develop in these pores (typical radii: 0.005 –0.02 µm). In torus-margo pits, water flows through the permeable and elastic margo. (b) Pit membrane of *Sambucus nigra*, top view. Scanning electron microscope (SEM) picture of ethanol-dried material. (c) Pit of *Laurus nobilis*, cross-section. SEM picture of ethanol-dried material. (e) Pit with torus, top view, *Abies alba*. SEM picture of ethanol-dried material. (f) Top view of pits of *Pinus sylvestris*. The two pits on the left show closed pits, with the tori pressed to the pit aperture, whereas the two pits on the right show the pit aperture (pit membranes were removed during preparation). The relief of the two tori indicates the pit apertures. This effect is due to the still hydrated state of the tori, made possible by the CryoSEM technique. Additionally, the upper torus is positioned 'off-center'. This possibly illustrates a reason for air-seeding: tori not covering the aperture completely. During embolism, the flowing water pushes the impermeable torus against the pit opening closing effectively the aperture. Illustrations (a) and (d) are redrawn from Esau (1960).

$$\Delta p = \frac{2\gamma}{r_p} \approx 7\,\text{MPa} \ldots 28\,\text{MPa} \qquad (12)$$

This should be sufficient to isolate an embolized conduit segment from its intact neighbors. The nature of pit membranes is still under debate. In particular, there is evidence that the pit membranes are covered by a hydrogel (Pesacreta et al. 2005, Lee et al. 2012).

Diffusional equilibrium and dissolution of floating bubbles

The dynamic behavior of bubbles of radius R is now briefly considered. Conventionally, the absence of mechanical equilibrium is described by the so-called Rayleigh–Plesset (RP) equation, which is derived from the Navier–Stokes equation for an incompressible fluid flow assuming spherical symmetry (Rayleigh 1917, Plesset 1949). It is given by

$$\frac{p - p_s}{\rho} = R\frac{d^2R}{dt^2} + \frac{3}{2}\left(\frac{dR}{dt}\right)^2 + \frac{4\nu}{R}\frac{dR}{dt} + \frac{2\gamma}{\rho R} \qquad (13)$$

where $p = p_a + p_w$ is the total gas pressure in the bubble (air plus saturated water vapor) assumed to be uniform, p_s is, as before, the liquid water pressure far from the bubble and can vary in time t, ρ and ν are the density and kinematic viscosity of water far from the bubble location, γ is the surface tension of the bubble, and $R(t)$ is a time-varying bubble radius. The RP

equation (Eq. (13)) assumes isothermal conditions so that temperature differences between the gas and liquid phases are not significant (i.e., the bubble-liquid system is in thermal but not necessarily mechanical or air mass equilibrium). At mechanical equilibrium, the RP equation can be simplified by setting $dR/dt = 0$ and the Young–Laplace equation is recovered. As noted earlier, the time scale associated with exchanges of air molecules between an isolated bubble and the surrounding water is assumed to be sufficiently slow compared with those associated with mechanical forces described by the RP. For example, the molecular diffusion coefficient of air in water is on the order of $10^{-9}\,m^2\,s^{-1}$ whereas the kinematic viscosity of water $\nu/\rho = 10^{-6} m^2 s^{-1}$. This contrast results in an air diffusional time scale that is 10^3 times larger than the viscous time scales in the RP equation. Hence, for purposes of determining time scales of air molecules diffusing into or out of a cavity in water, the forces acting on the bubble are presumed to have attained mechanical equilibrium sufficiently fast though corrections to it can be carried out using the RP equation if such refinements are warranted (Plesset and Prosperetti 1977, Brennen 2013). With this background, the dynamic behavior of a floating bubble exchanging air molecules with the surrounding liquid is now considered assuming both mechanical and thermal equilibrium. This exchange rests upon two physical effects (see Figure 7):

(i) At the bubble's air/water interface, air particles constantly either dissolve into or escape from the water. As a consequence of this intensive exchange, the (partial) pressure p_a of the air inside the bubble and the concentration C_R of the dissolved air particles in the liquid in the near vicinity of the bubble are proportional to each other and given by Henry's Law:

$$C_R = k_H p_a \tag{14}$$

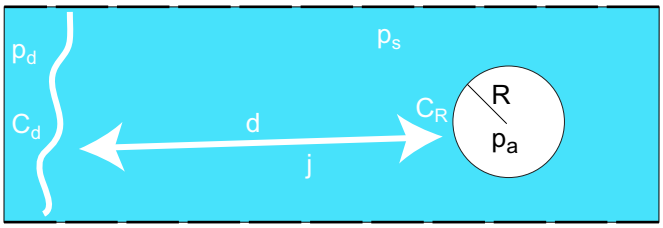

Figure 7. Diffusional fluxes of air molecules between bubble and xylem water. p_a designates the partial pressure of air molecules in the bubble and C_R is the concentration of air molecules that dissolve in water close to the bubble, according to Henry's Law, $C_R = k_H p_a$. The fictitious pressure p_d represents the concentration C_d of air molecules dissolved in the xylem water at distance d from the bubble. It is defined in analogy to Henry's Law via $C_d = k_H p_d$. $p_a < p_d$ causes a diffusional flux j into the bubble. For $p_a > p_d$, air molecules leave the bubble and dissolve in the xylem water.

The value of the constant k_H depends on the gas and liquid species involved.

(ii) If the concentration C_R of dissolved gas particles close to the bubble deviates from the value C_d farther away in the liquid, diffusional currents, directed from areas of higher to areas of lower concentration, arise.

As the combined result of both processes, air particles are transported either out of and away from the gas bubble or into the opposite direction until a diffusional equilibrium situation between C_R and C_d is attained. To facilitate this notion further and in analogy to Henry's Law, a (fictitious) air pressure in water away from the bubble is defined as

$$p_d := \frac{C_d}{k_H} \tag{15}$$

Employing this definition the situation of diffusional (or exchange) equilibrium can be characterized by the equality

$$p_d = p_a \tag{16}$$

The Young–Laplace- equation (derived from the RP equation by setting $dR/dt = 0$) is now used to link p to p_s

$$p = p_s + \frac{2\gamma}{R} \tag{17}$$

Splitting the gas pressure into the partial pressures of water vapor and air according to $p = p_w + p_a$ we find from Eq. (17) for bubbles in approximate mechanical equilibrium that

$$p_a = p - p_w = p_s - p_w + \frac{2\gamma}{R} \tag{18}$$

Observing that this relation establishes a one-to-one correspondence between p_a and R, Eq. (16) is used to define an equilibrium bubble radius

$$R_{eq} := \frac{2\gamma}{p_d + p_w - p_s} \tag{19}$$

Here, R_{eq} defines an equilibrium with respect to the exchange of air particles between the bubble and the surrounding water whereas the radii R_{stab} and R_{inst} (defined in Eq. (10)) represent equilibria with respect to the mechanical forces that expand or contract the bubble.

Combining Eqs. (10) and (18), the behavior of gas bubbles in mechanical equilibrium but not with respect to exchange of air particles between the bubble and surrounding water can now be understood (consult Figure 8): an air molecular exchange equilibrium exists if $p_a = p_d$ is realized. (In the lower part of Figure 8, this case is indicated by the intersections between the broken, horizontal lines and the $p_a(R)$-curve at $(R_{eq,1}, p_{d,1})$ and $(R_{eq,2}, p_{d,2})$.) Depending on whether R_{eq} lies in the interval $0 < R_{crit}$ or in $R_{crit} < R_{vap}$, the bubble goes through qualitatively different developments:

(i) $R_{crit} < R_{eq}$ (cf. Figure 8a): if the bubble starts at position A (to the left of R_{crit}) the inequality $p_a > p_d$ is valid, causing air particles to leave the bubble. This loss entails a contraction of the bubble (as can be seen from the $n_a(R)$ diagram in the upper part of the figure), which raises in turn the bubble's partial air pressure p_a. This accelerates the particle loss and so on, until the bubble has dissolved.

If the bubble starts at position C (between R_{crit} and $R_{eq,2}$), $p_a > p_d$ causing air particles to leave the bubble, the bubble responds by an expansion according to the $n_a(R)$ diagram. The bubble's partial air pressure p_a decreases whereupon smaller numbers of air particles leave the bubble and so on. This process slows down but continues until $p_a = p_d$ is achieved.

If the bubble starts at position D, $p_a < p_d$, air particles enter the bubble. The bubble reacts by a volume contraction. The bubble's partial air pressure p_a increases whereupon less air particles enter the bubble and so on until $p_a = p_d$ is achieved.

(ii) $R_{eq} < R_{crit}$ (cf. Figure 8b): if the bubble starts at position A the same reasoning as in Figure 8a applies.

If the bubble starts at position B (between $R_{eq,1}$ and R_{crit}), $p_a < p_d$. Now air particles from the surrounding water enter the bubble, which then reacts by an expansion according to the $n_a(R)$ diagram. The bubble's partial air pressure p_a decreases whereupon still more air particles enter the bubble and so on. This process continues either until n_a exceeds n_{crit} (and the bubble bursts) or until all air particles within the xylem water have assembled in the bubble.

If the bubble starts at position D, $p_a < p_d$ causing air particles to enter the bubble. The bubble reacts by a contraction towards R_{crit} where the bubble bursts.

Obviously, equilibria with respect to the exchange of air particles related to a bubble radius R_{eq} lying within the interval $0 < R_{eq} < R_{crit}$ are unstable, similar equilibria within $R_{crit} < R_{eq} < R_{vap}$ are, however, stable.

Hence, stable mechanical and exchange equilibria preclude each other: for $0 < R < R_{crit}$, the mechanical equilibrium is stable and the exchange equilibrium is unstable. For $R_{crit} < R < R_{vap}$, it is the other way round. The different time scales on which the processes connected with the two equilibria operate impose a clear hierarchy on their relevance: since the exchange of air particles is a very slow process, compared with the action of the expanding and contracting forces, a mechanically unstable bubble with $R_{inst}(n_a)$ has negligible chances to settle down to a stable exchange equilibrium. It is much more probable that it either bursts or shrinks to the corresponding stable radius $R_{stab}(n_a)$ where an unstable exchange equilibrium awaits it. Depending on the relation between p_a and p_d this state will finally develop into a bubble burst due to congestion (i.e., $n_a > n_{crit}$) or to complete bubble dissolution.

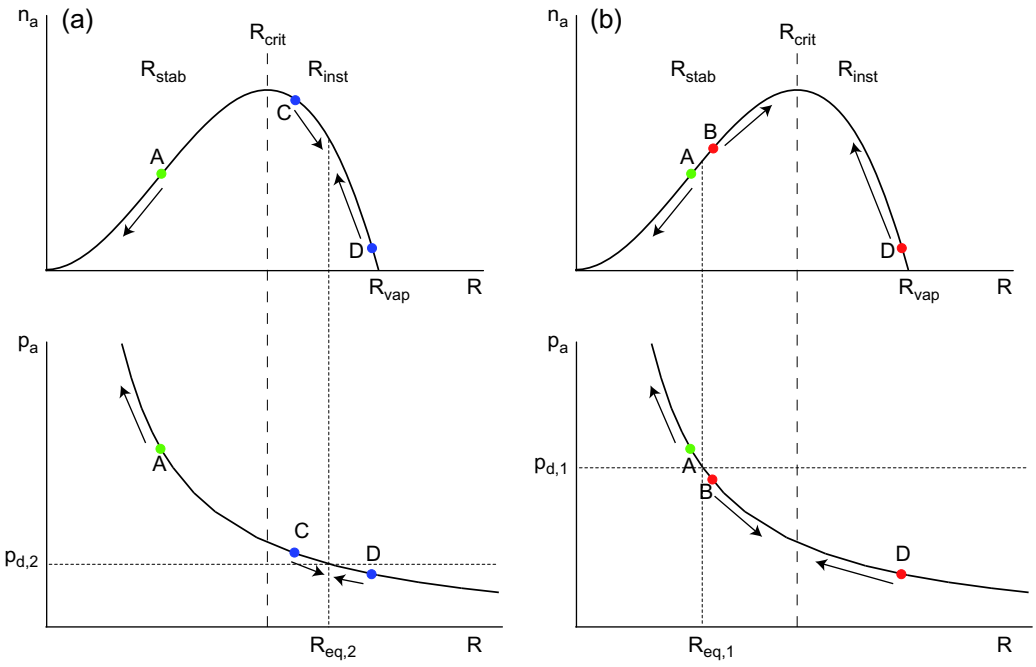

Figure 8. The behavior of gas bubbles that are in equilibrium with respect to mechanical forces but not with respect to exchange of air particles between bubble and surrounding water. Exchange equilibrium exists if $p_a = p_d$ is realized (p_a denotes the partial pressure of air molecules in the bubble, the fictitious pressure p_d represents the concentration C_d of air molecules dissolved in the xylem water close to the bubble). In the lower parts of the figures, these cases are indicated by the intersections between the broken, horizontal lines and the $p_a(R)$-curve at ($R_{eq,1}$, $p_{d,1}$) and ($R_{eq,2}$, $p_{d,2}$). Depending on whether R_{eq} lies in the interval $R_{crit} < R_{vap}$ (subfigure (a)) or in $0 < R_{crit}$ (subfigure (b)), the bubble goes through qualitatively different developments, explained in the text.

These observations imply a condition that guarantees that bubble dissolution occurs: bubbles represented by position A in Figure 8 are in stable mechanical equilibrium and lose air to the surrounding water, expressed by the relations $R < R_{crit}$ and $p_a > p_d$, or, by the equivalent inequality

$$R_{eq} > R_{crit} \tag{20}$$

Upon insertion of the definitions in Eqs (11), (19) and (15) this condition can be reformulated as a relation between the concentration C_d of gas particles dissolved in the surrounding liquid, the (negative) pressure p_s of this liquid, and the water vapor saturation pressure p_w

$$C_d = k_H p_d < \frac{k_H}{2}(p_w - p_s) \tag{21}$$

Solving this relation for p_s yields

$$p_s < -2p_d + p_w \tag{22}$$

Since soil water and xylem sap are in contact with air at atmospheric pressure, it is reasonable to assume $p_d \approx p_{atmosphere} \approx 10^{-1}$ MPa. Neglecting the term p_w on the right-hand side (at 25 °C we find $p_w \approx$ ~3167 Pa $< < 10^{-1}$ MPa $\approx p_d$) Eq. (22) reduces to

$$p_s \lessapprox -2 \times 10^{-1}\,\text{MPa} = -2 \times p_{atmosphere} \tag{23}$$

Hence, if the condition of Eq. (23) is fulfilled, embryonic bubbles appearing in the stability region depicted in Figure 4 dissolve after a while in the surrounding water and do no harm.

Implications of xylem functionality to phloem transport

As earlier noted, sugars produced from photosynthesis are transported to distal parts of the plant by bulk flow through the phloem, an interconnected system of cellular conduits that link essentially all parts of the plant. In addition to sugar transport, the phloem plays a role in transport of signaling molecules. Sugars are exported from the leaf by bulk liquid flow through phloem sieve elements. Sieve elements are approximately cylindrical, of radius $r = 1\,\mu$m to $10\,\mu$m and length $l = 0.1$ mm to 1 mm. The cellular conduits are connected end-to-end (and in some cases radially) by sieve plates, modified cell walls perforated by numerous enlarged plasmodesmata pores of radius $r_p = 0.1\,\mu$m to $1\,\mu$m (Jensen et al. 2012). The phloem conduits carry a sap that contains about 20% sugar by weight (Jensen et al. 2013), and the average flow speeds are in the range of $v \sim 25\,\mu\text{m s}^{-1}$ to $250\,\mu\text{m s}^{-1}$ (~0.1 m h^{-1} to 1 m h^{-1}), resulting in low-Reynolds-number flow conditions dominated by viscous effects (Jensen et al. 2012). The flow is driven by osmotic pressure differences between sources (i.e., leaf) and sinks (assigned here to roots though sinks can span other plant organs). Phloem sap contains numerous compounds, but as earlier noted, the primary determinant of phloem pressure are concentration of sugars and small ions (Jensen et al. 2016).

Phloem transport relies on the osmotic exchange of water with the xylem system, and the conditions in the xylem have a direct impact on phloem flow (Figure 1) (Sevanto 2014, 2018, Stroock et al. 2014, Huang et al. 2018) as earlier noted. The cellular conduits — and the total conductive area — of the phloem, however, is significantly smaller than the xylem, hence the feedback appears to act primarily in one way: phloem flow is impacted by conditions in the xylem, but not vice versa. The impact of xylem pressure on phloem concentration, sap viscosity and carbohydrate allocation patterns are discussed here.

Impact of xylem pressure on phloem solute concentration

The impact of xylem pressure on solute concentration is considered as follows. Thermal and chemical equilibrium between phloem and xylem requires that the water potentials $\psi_p := p_p - \Pi_p + p_g$ and $\psi_s := p_s - \Pi_s + p_g$ of phloem and xylem, respectively, are equal. Here, p_p (Pa) is the (positive) hydrostatic pressure in the phloem, p_s (Pa) is the (negative) hydrostatic pressure in the xylem, p_g is the gravitational potential (as in Eq. (1)) and $\Pi_{p,s}$ denotes the osmotic potential in the two tissues.

Assuming dilute solutions and a negligible concentration in xylem sap, the equality $\psi_p = \psi_s$ simplifies to

$$p_p - \mathcal{R}Tc_p = p_s \tag{24}$$

where c_p (mol m^{-3}) is the osmolyte concentration in the phloem, $\mathcal{R}$ (J K mol^{-1}) is the gas constant, and T (K) is temperature. For clarity, the van't Hoff approximation for the osmotic pressure $\Pi \sim \mathcal{R}Tc$ is used, which is accurate in the low-concentration regime ($c_p < 500$ mol/m^3), and acceptable at higher concentrations.

Applying Eq. (24) to the source (at $x = 0$ in Figure 1) and to the sink (at $x = L$) the pressure difference Δp_p between source and sink available to drive phloem flow is

$$\Delta p_p = \mathcal{R}T\Delta c_p + \Delta p_s \tag{25}$$

Note that xylem pressure drop $\Delta p_s = p_s(0) - p_s(L)$ is negative whereas the difference $\Delta c_p = c_p(0) - c_p(L)$ of solute concentration in the phloem is positive: because sugars are unloaded in the sink region ($x = L$), the solute concentration there is significantly lower than in the source tissue ($x = 0$), that is, $c_p(0) \gg c_p(L)$ and $\Delta c_p = c_p(0) - c_p(L) \approx c_p(0)$. Due to the different signs of Δp_s and Δc_p the pressure difference Δp_p between source and sink can, at least in principle, become negative, which indicates that the phloem sap flows within the phloem network in the wrong direction, thus cutting parts of the plant from the supply with assimilates

A similar 'reversed flow' may occur between phloem and xylem: in the source area, the water that is loaded in the phloem with assimilates is drawn from the xylem; therefore, around

$x = 0$, the water potentials in phloem and xylem should be related according to

$$\psi_p(0) \approx p_p(0) - \mathcal{R}Tc_p(0) \lessapprox p(0) \approx \psi_s(0) \quad (26)$$

(with the approximations used in Eq. (24)). Failing this, such a 'reversed flow' is likely to cause impairment of the phloem system. The xylem may not benefit from this additional water subsidy originating from the phloem given its small volume compared with the xylem. Hence, the xylem pressure that leads to such flow reversal in the phloem may be used to finger-print severe drought conditions in the plant.

The approximation $c_p(0) \gg c_p(L)$ simplifies Eq. (25) to

$$\Delta p_p = \mathcal{R}Tc_p(0) + \Delta p_s \quad (27)$$

The flow rate Q in the phloem, and hence the rate of energy transport, is directly proportional to the pressure drop Δp_p, i.e.,

$$Q = \frac{\Delta p_p}{R_p} \quad (28)$$

where R_p is the hydraulic resistance in the phloem. Assuming that the organism strives to keep Q at a constant level to maintain metabolism implies that Δp_p should remain unchanged. This leads to an expression for the phloem osmolyte concentration c_p as a function of xylem pressure drop

$$c_p = \frac{\Delta p_p - \Delta p_s}{\mathcal{R}T} \quad (29)$$

A pressure drop of approximately $\Delta p_p \sim 1$ MPa is required to maintain phloem transport in a moderately sized tree (Jensen 2018). If xylem tension is negligible compared to Δp_p, a concentration of $c_p = 400\,\text{mol m}^{-3}$ is required to maintain sap flow (Eq. (29), see also Figure 9a). In tall trees, the xylem pressure drop due to gravitational potential alone can reach $\Delta p_s = -1.2$ MPa (Eq. (1)), corresponding to $c_p = 880\,\text{mol/m}^3$. Viscous friction to flow in the stem and soil further decreases the pressure in the xylem, with values reported in the range from $\Delta p_s = -2$ MPa to -8 MPa (Stroock et al. 2014, Sevanto 2018). This corresponds to osmolarities in the range $c_p \sim 1000$ mol m^{-3} to 3000 mol m^{-3}. Such concentration interval is beyond most of the observed sugar concentrations in both passive and active loaders (Figure 9b and c). It can be surmised that other osmolytes contribute to phloem transport beyond sucrose.

Impact of xylem pressure on phloem sap viscosity

The preceding discussion highlighted the effect of xylem tension on phloem sap concentration: As xylem tension Δp_s increases, the osmolyte concentration c_p must also increase to keep energy transport rates constant (Eq. (29)). Solute concentration, however, affects not only the osmotic potential Π, but also the viscosity η (Pa) of the solution (Lang 1978, Hölttä et al. 2006, Jensen et al. 2013, Sevanto 2018). For instance, the viscosity of 3000 mol m^{-3} sucrose solution is ~1000 times greater than pure water (Figure 10a). By contrast, an osmotically equivalent solution of small ions (such as NaCl) is only ~1.3 times more viscous (Figure 10b).

The increase in viscosity η with phloem solute concentration c_p has a direct negative impact on the transport rate Q (Eq. (28)). For a cylindrical tube of length L and radius a, the flow rate/pressure-drop relation (the Hagen–Poiseuille law) is, as before,

$$Q = \frac{\pi a^4}{8\eta L}\Delta p_p \quad (30)$$

i.e., the flow rate Q scales as $1/\eta$. Even at moderate phloem sugar content, the assumption that equal pressures generate equal flows is thus violated (Eq. (28)), and unrealistically large sugar concentrations would be needed to drive sugar transport if this was the sole osmolyte.

To further highlight the difference between the case where either sugars or other osmolytes drive transport, we proceed to consider the sugar current $I = Qc_s$ (mol s^{-1}), where c_s is the phloem sugar concentration at the source. If sugar is the main osmolyte responsible for transport, then $c_p = c_s$ and the current is quadratic in c_s, c.f. Eqs. (30) and (29):

$$I \sim \frac{c_s^2}{\eta(c_s)} \quad (31)$$

Here, a relatively small xylem tension is assumed for simplicity ($\Delta p_s \ll \Delta p_p$) and thus the phloem pressure drop is $\Delta p_p \sim \mathcal{R}Tc_p$ from Eq. (29). The transport rate I in Eq. (31) peaks at $c_s \sim 1200\,\text{mol/m}^3$ (Figure 11a), significantly above the mean sap sugar content observed in both active and passive loaders (Figure 9b and c). If, by contrast, a different osmolyte is driving transport, the pressure difference Δp_p is independent of c_s and the current scales linearly with c_s:

$$I \sim \frac{c_s}{\eta(c_s)} \quad (32)$$

The transport rate in Eq. (32) peaks at $c_s \sim 800$ mol m^{-3} (Figure 11b), relatively close to the mean sap sugar content observed in both active and passive loaders (Figure 9b and c).

In summary, osmolyte concentration needed to drive phloem flow depends on the xylem water status. As xylem tension increases, the phloem concentration must increase dramatically (Eq. (29), Figure 9). The sharp increase in viscosity with sugar concentration makes it likely that other smaller solutes contribute to the osmolarity of phloem sap thereby increasing the concentration without increasing appreciably the viscosity (Figure 10).

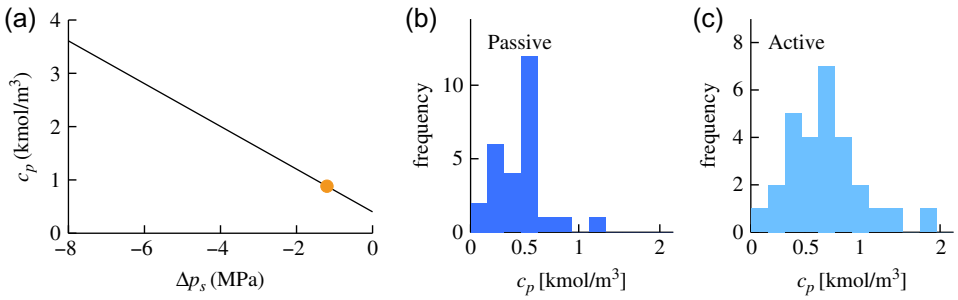

Figure 9. Impact of xylem conditions on phloem transport. (a) Osmolyte concentration c_p required to drive phloem flow as function of xylem pressure drop Δp_s (Eq. (29), plotted for $\Delta p_p = 1$ MPa and $T = 300$ K). The orange dot indicates the maximum tension $\Delta p_s = -1.2$ MPa due to gravitational effects (Eq. (1)). (b) Observed phloem sugar concentration c_p in passive loaders. (c) Observed phloem sugar concentration c_p in active loaders. The vertical axes in (b) and (c) indicate the number of species in each horizontal bin. Data from Jensen et al. (2013).

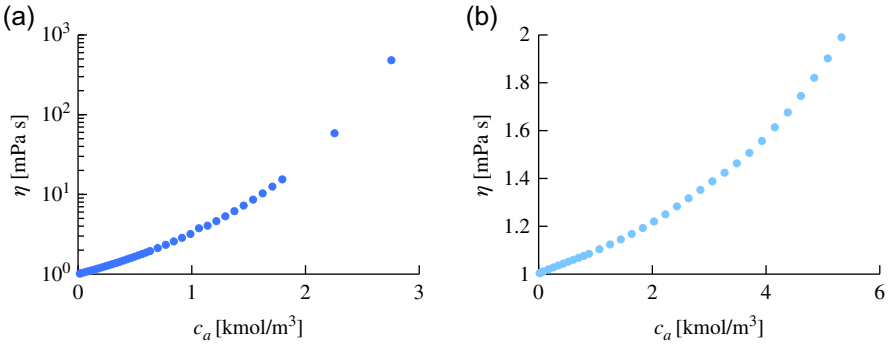

Figure 10. Impact of xylem conditions on phloem sap viscosity. (a) Aqueous sugar solution viscosity η plotted as function of sucrose concentration c_p. The viscosity increases with concentration. The effect is less pronounced for small ions such as the NaCl solution shown in panel (b). The limit $c_p = 0$ corresponds to pure water. The solution viscosity is strongly affected by the presence of large sugar molecules, less so by small ions. Data from Haynes (2014).

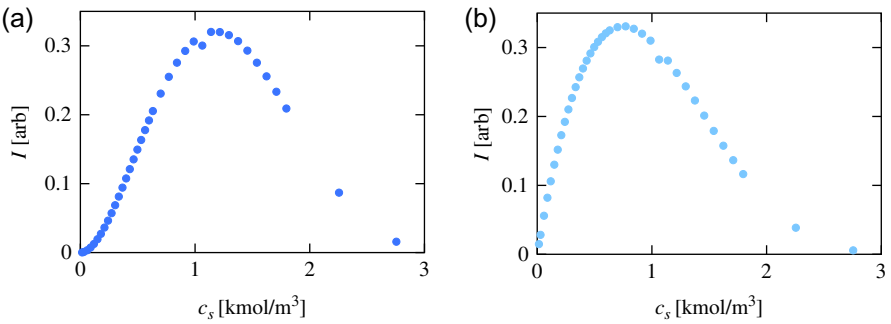

Figure 11. Impact of sap viscosity on sugar transport. (a) Sugar current I as a function of sap sugar concentration c_s, assuming that sugar is the primary osmolyte (Eq. (31)). (b) Sugar current I plotted as a function of sap sugar concentration c_s, assuming that sugar is not the primary osmolyte (Eq. (31)). Data from Haynes (2014).

Impact of drought on xylem and phloem transport

The flow rate Q_s of xylem sap is, similar to in the phloem case, Eq. (28), proportional to the pressure drop Δp_s between $x = 0$ and $x = L$ (cf. Figure 1)

$$Q_s = -\frac{\Delta p_s}{R_s} \tag{33}$$

where R_s is the hydraulic resistance of the xylem and the minus sign ensures that upward flow in the xylem is counted positive. The assumption $\Pi_s \approx 0$ of negligible osmotic potential in xylem sap implies $\Delta p_s \approx \Delta \psi_s = \psi_s(0) - \psi_s(L) < 0$ for the water potential.

Assuming further that (i) R_s is not affected appreciably by drought and (ii) the plant maintains $\psi_s(0)$ approximately constant, changes in Δp_s are primarily due to the impact of drought

on soil moisture, respective soil water potential $\psi_s(L) \approx p_s(L)$. Experimentally obtained vulnerability curves (Manzoni et al. 2014) and theoretical considerations based on models of the xylem pathway between soil and atmosphere (Manzoni et al. 2014, Huang et al. 2017, 2018) corroborate these assumptions: (i) usually, the operating pressure in the xylem rarely drops below the point, labeled ψ_{12}, where R_s increases by only 12%, and (ii) the plant maintains $\psi_s(0)$ approximately constant at a value that sustains maximum transpiration rate without damaging the xylem. Studies conducted to contrast isohydric and anisohydric behavior (Kolb and Sperry 1999, Sperry et al. 2002, Schultz 2003, McDowell et al. 2008) reported that species with larger ψ_{12} tend to exhibit more isohydric behavior while anisohydric behavior occurs in species with smaller ψ_{12}. Thus, as long as soil water potential $\psi_s(L)$ remains in the interval $\psi_{PWP} \lessapprox \psi_s(L) \lessapprox \psi_{FC}$ (defined by the permanent wilting point, $\psi_{PWP} \approx -1.5$ MPa, and the water potential related to field capacity, typically $\psi_{FC} \approx -0.006$ MPa to -0.03 MPa, depending on soil composition and structure), most plants can sustain phloem function during drought (Sevanto et al. 2014, Sevanto 2018). It is to be noted that a naïve juxtaposition of phloem dysfunction to plant mortality cannot be realistic without other considerations (growth, respiration costs, and resistance to pests and diseases.)

However, coupling of xylem and phloem transport as outlined above, mitigates the consequences of drought in two ways:

- If a drought sets in, the aforementioned assumptions imply that soil water potential, the difference Δp_s and, according to Eq. (33), xylem sap flow rate Q_s decreases, that is, the plant economizes on water consumption from the soil as expected.
- As has been pointed out above, phloem transport breaks down if Δp_p becomes negative, which can occur if $\Delta p_s < 0$ on the right-hand side of Eq. (25) or (27) outweighs the (always positive) concentration term. The decrease of Δp_s caused by a progressive drought precludes such a development: if the plant production of assimilates is approximately unaffected by the drought (that is, $c_p(0) \approx$ const.) the decrease of Δp_s causes an increase in Δp_p, the driving force of phloem transport, and also an increase in the phloem flow rate Q, according to Eq. (28).

Discussion and future outlook

This review focused on the physical transport processes in the xylem and phloem systems as well as their coupling through xylem pressure. The goal was to mathematically describe and evaluate the biophysical basis of the main transport laws that can then be used (or upscaled) to devise coupled soil–xylem–leaf–phloem approaches. Attempts to carry out such an exercise are beginning to proliferate in the literature (see, e.g., Huang et al. 2018). There is a growing body of literature highlighting the need for accounting for simultaneous xylem and phloem constraints on stomatal conductance g_s and corollary variables. This need is driven by immediate problems such as the effects of droughts, elevated atmospheric CO_2 and temperature, or nutrient amendments on gas exchanges with the atmosphere and plant health (Mencuccini and Hölttä 2010, Nikinmaa et al. 2013, Sevanto et al. 2014, Hölttä et al. 2017, Huang et al. 2018). The xylem section here focused on connections between xylem water pressure, bubble dynamics and their stability, and key anatomical traits. The next immediate step is to establish upscaled equations from the aforementioned formulation that predict the shape of the so-called vulnerability curves (VC). The VC features loss in plant (or branch) hydraulic conductance with decreasing amount of water available in the soil or plant. Despite the significance of VCs, linkages between anatomical pit-level (microscopic) properties and stem-level (macroscopic) hydraulic response to drought remains a subject of inquiry and is virtually required when quantifying drought-induced mortality in trees or coupling xylem to phloem at a macroscopic level. The time is ripe for such an advance given the rapid development of measuring techniques for VCs and the capacity to image plant anatomical traits at unprecedented resolution.

Theoretical challenges, partly highlighted in this review, are the multi-scaled nature of xylem transport. Size distributions of length and diameters of conduits range from 10^{-3} m to 10^{-1} m and 10^{-4} m to 10^{-2} m, respectively, whereas pit scale size distributions that include diameter of pores span 10^{-9} m to 10^{-7} m and that of the pit membranes containing them are three orders of magnitudes larger. Because hydraulic failure is impacted by processes acting on all these scales, up-scaling from bubble-scale to plant-level while accommodating all the anatomical traits requires novel theoretical and modeling tactics that are still in development. The work here also highlighted that xylem pressures have disproportionate impact on phloem transport (but not the converse) through multiple mechanisms, few of which have been discussed.

The next steps are links between the carbon and water economies of plants that require combining the biochemical demand for atmospheric CO_2 with gas transfer through stomates, liquid water transport in the soil–xylem hydraulic system and sucrose export in the phloem such as the ones covered here. A number of attempts (Hunt and Manzoni 2015, Huang et al. 2018) are currently underway to complete such coupling and are likely to benefit from the material covered here. The details of this coupling are best kept for a future review.

Acknowledgments

The authors also thank Stefano Manzoni for all the helpful comments and Birgit Binder, Entringen, for drawing Figures 2a, 2b, 5a, 5b, 6a and 6d.

Conflict of interest

None declared.

Funding

K.H.J. was supported by a research grant (13166) from VILLUM FONDEN. G.K. acknowledges support from the US National Science Foundation, Grant/Award Numbers: NSF-AGS-1644382, NSF-DGE-1068871, NSF-EAR-1344703, NSF-IOS-1754893.

References

Adamson AW, Gast AP (1997) Physical chemistry of surfaces. Wiley-Interscience, Hoboken, NJ, USA.

Berthelot M (1850) Sur quelques phénomènes de dilatation forcée des liquides. Ann Chim Phys 30:32–237.

Brennen CE (2013) Cavitation and bubble dynamics. Cambridge, UK: Cambridge University Press.

Brodersen CR, McElrone AJ, Choat B, Matthews MA, Shackel KA (2010) The dynamics of embolism repair in xylem: in vivo visualizations using high-resolution computed tomography. Plant Physiol 154:1088–1095.

Brodersen CR, Knipfer T, McElrone AJ (2018) In vivo visualization of the final stages of xylem vessel refilling in grapevine (*Vitis vinifera*) stems. New Phytol 217:117–126.

Brodribb TJ, Carriqui M, Delzon S, Lucani C (2017) Optical measurement of stem xylem vulnerability. Plant Physiol 174:2054–2061.

Brown HR (2013) The theory of the rise of sap in trees: some historical and conceptual remarks. Phys Perspect 15:320–358.

Chapman D, Rand R, Cooks J (1977) A hydrodynamical model of bordered pits in conifer tracheids. J Theor Biol 67:11–24.

Choat B, Ball M, Luly J, Holtum J (2003) Pit membrane porosity and water stress-induced cavitation in four co-existing dry rainforest tree species. Plant Physiol 131:41–48.

Clearwater M, Clark C (2003) In vivo magnetic resonance imaging of xylem vessel contents in woody lianas. Plant Cell Environ 26: 1205–1214.

Cochard H, Badel E, Herbette S, Delzon S, Choat B, Jansen S (2013) Methods for measuring plant vulnerability to cavitation: a critical review. J Exp Bot 64:4779–4791.

Cochard H, Delzon S, Badel E (2015) X-ray microtomography (micro-CT): a reference technology for high-resolution quantification of xylem embolism in trees. Plant Cell Environ 38:201–206.

Cotta H (1806) Naturbeobachtungen über die Bewegung und Funktion des Saftes in den Gewächsen: mit vorzüglicher Hinsicht auf Holzpflanzen. Hoffmannsche Buchhandlung, Weimar.

Debenedetti PG (1996) Metastable liquids: concepts and principles. Princeton University Press, Princeton, NJ.

Dixon HH (1914) Transpiration and the ascent of sap in plants. Basingstoke, UK: Macmillan and Company, LTD.

Dixon HH, Joly J (1894) On the ascent of sap. Proc R Soc Lond 57:3–5.

Esau K (1960) Anatomy of seed plants. Soil Sci 90:149.

Floto F (1999) Stephen Hales and the cohesion theory. Trends Plant Sci 4:209.

Haberlandt G (1914) Physiological plant anatomy. London: Macmillan and Company.

Hacke UG, Sperry J (2003) Limits to xylem refilling under negative pressure in *Laurus nobilis* and *Acer negundo*. Plant Cell Environ 26:303–311.

Haynes WM (2014) CRC handbook of chemistry and physics. Boca Raton, US: CRC press.

Holbrook NM, Zwieniecki MA (1999) Embolism repair and xylem tension: do we need a miracle? Plant Physiol 120:7–10.

Holbrook NM, Ahrens ET, Burns MJ, Zwieniecki MA (2001) In vivo observation of cavitation and embolism repair using magnetic resonance imaging. Plant Physiol 126:27–31.

Hölttä T, Vesala T, Sevanto S, Perämäki M, Nikinmaa E (2006) Modeling xylem and phloem water flows in trees according to cohesion theory and Münch hypothesis. Trees 20:67–78.

Hölttä T, Lintunen A, Chan T, Mäkelä A, Nikinmaa E (2017) A steady-state stomatal model of balanced leaf gas exchange, hydraulics and maximal source-sink flux. Tree Physiol 37:851–868.

Hopkins W, Huner N (2004) Cells, tissues, and organs: The architecture of plants. In: Hopkins WG, Huner NPA (eds) Introduction to plant physiology. John Wiley and Sons, Inc., Hoboken, NJ, pp 1–28

Huang C-W, Domec J-C, Ward EJ, Duman T, Manoli G, Parolari AJ, Katul GG (2017) The effect of plant water storage on water fluxes within the coupled soil-plant system. New Phytol 213:1093–1106.

Huang C-W, Domec J-C, Palmroth S, Pockman WT, Litvak ME, Katul GG (2018) Transport in a coordinated soil-root-xylem-phloem leaf system. Adv Water Resour 119:1–16.

Hunt AG, Manzoni S (2015) The physics of geobiology and geochemistry. San Rafael, US: Morgan & Claypool Publishers.

Jaeger FM (1892) Sitzb. Akad. Wiss. Wien (2a), 101:945.

Jensen KH (2018) Phloem physics: mechanisms, constraints, and perspectives. Curr Opin Plant Biol 43:96–100.

Jensen KH, Mullendore DL, Holbrook NM, Bohr T, Knoblauch M, Bruus H (2012) Modeling the hydrodynamics of phloem sieve plates. Front Plant Sci 3:151.

Jensen KH, Savage JA, Holbrook NM (2013) Optimal concentration for sugar transport in plants. J R Soc Interface 10:20130055.

Jensen KH, Berg-Sørensen K, Bruus H, Holbrook NM, Liesche J, Schulz A, Zwieniecki MA, Bohr T (2016) Sap flow and sugar transport in plants. Rev Mod Phys 88:035007.

Kenrick P, Crane PR (1997) The origin and early diversification of land plants. A cladistic study, Vol. 560. Smithsonian Institute Press, Washington DC.

Kolb K, Sperry JS (1999) Transport constraints on water use by the Great Basin shrub, *Artemisia tridentata*. Plant Cell Environ 22:925–936.

Konrad W, Roth-Nebelsick A (2003) The dynamics of gas bubbles in conduits of vascular plants and implications for embolism repair. J Theor Biol 224:43–61.

Lang A (1978) A model of mass flow in the phloem. Funct Plant Biol 5: 535–546.

Larcher W (2003) Physiological plant ecology: ecophysiology and stress physiology of functional groups. Luxembourg: Springer Science & Business Media.

Lee J, Holbrook NM, Zwieniecki MA (2012) Ion induced changes in the structure of bordered pit membranes. Front Plant Sci 3:55.

Lucas WJ, Groover A, Lichtenberger R et al. (2013) The plant vascular system: evolution, development and functions f. J Integr Plant Biol 55: 294–388.

Manzoni S, Katul G, Porporato A (2014) A dynamical system perspective on plant hydraulic failure. Water Resour Res 50:5170–5183.

Maris H, Balibar S (2000) Negative pressures and cavitation in liquid helium. Phys Today 53:29.

McDowell N, Pockman WT, Allen CD et al. (2008) Mechanisms of plant survival and mortality during drought: why do some plants survive while others succumb to drought? New Phytol 178: 719–739.

Mencuccini M, Hölttä T (2010) The significance of phloem transport for the speed with which canopy photosynthesis and belowground respiration are linked. New Phytol 185:189–203.

Nardini A, Gullo MAL, Salleo S (2011) Refilling embolized xylem conduits: is it a matter of phloem unloading? Plant Sci 180:604–611.

Nardini A, Savi T, Losso A et al. (2017) X-ray microtomography observations of xylem embolism in stems of *Laurus nobilis* are consistent with

hydraulic measurements of percentage loss of conductance. New Phytol 213:1068–1075.
Nikinmaa E, Hölttä T, Hari P, Kolari P, Mäkelä A, Sevanto S, Vesala T (2013) Assimilate transport in phloem sets conditions for leaf gas exchange. Plant Cell Environ 36:655–669.
Oertli J (1971). Stability of water under tension in the xylem. Zeitschrift fur Pflanzenphysiologie.
Pesacreta TC, Groom LH, Rials TG (2005) Atomic force microscopy of the intervessel pit membrane in the stem of *Sapium sebiferum* (Euphorbiaceae). IAWA J 26:397–426.
Pickard WF (1981) The ascent of sap in plants. Prog Biophys Mol Biol 37:181–229.
Plesset MS (1949) The dynamics of cavitation bubbles. J Appl Mech 16: 277–282.
Plesset MS, Prosperetti A (1977) Bubble dynamics and cavitation. Annu Rev Fluid Mech 9:145–185.
Raven J (2003) Long-distance transport in non-vascular plants. Plant Cell Environ 26:73–85.
Raven JA (1984) Physiological correlates of the morphology of early vascular plants. Bot J Linn Soc 88:105–126.
Raven JA (1993) The evolution of vascular plants in relation to quantitative functioning of dead water-conducting cells and stomata. Biol Rev 68:337–363.
Raven JA, Edwards D (2004) Physiological evolution of lower embryophytes: adaptations to the terrestrial environment. In: Alan RH, Imogen P (eds) The evolution of plant physiology. Elsevier, New York City, US, pp 17–41.
Raven JA, Edwards D (2014) Photosynthesis in early land plants: adapting to the terrestrial environment. Springer, Dordrecht, The Netherlands, pp 29–58.
Rayleigh L (1917) On the pressure developed in a liquid during the collapse of a spherical cavity. Philos Mag Ser 6:94–98.
Rockwell FE, Wheeler JK, Holbrook NM (2014) Cavitation and its discontents: opportunities for resolving current controversies. Plant Physiol 164:1649–1660.
Ryu J, Hwang BG, Kim YX, Lee SJ (2016) Direct observation of local xylem embolisms induced by soil drying in intact *Zea mays* leaves. J Exp Bot 67:2617–2626.
Salleo S, Gullo M, Paoli D, Zippo M (1996) Xylem recovery from cavitation-induced embolism in young plants of *Laurus nobilis*: a possible mechanism. New Phytol 132:47–56.
Schultz HR (2003) Differences in hydraulic architecture account for nearisohydric and anisohydric behaviour of two fieldgrown *Vitis vinifera* L. cultivars during drought. Plant Cell Environ 26:1393–1405.
Scott FM (1927) The botany of Marcello Malpighi, Doctor of Medicine. Sci Mon 25:546–553.
Sevanto S (2014) Phloem transport and drought. J Exp Bot 65: 1751–1759.
Sevanto S (2018) Drought impacts on phloem transport. Curr Opin Plant Biol 43:76–81.
Sevanto S, McDowell NG, Dickman LT, Pangle R, Pockman WT (2014) How do trees die? A test of the hydraulic failure and carbon starvation hypotheses. Plant Cell Environ 37:153–161.
Shen F, Gao R, Liu W, Zhang W (2002) Physical analysis of the process of cavitation in xylem sap. Tree Physiol 22:655–659.
Shen F, Wenji L, Rongfu G, Hu H (2003) A careful physical analysis of gas bubble dynamics in xylem. J Theor Biol 225:229–233.
Sitte P, Weiler E, Kadereit H, Bresinsky A, Körner C (2002). Strasburger, Lehrbuch der Botanik für Hochschulen. Springer Spektrum Berlin Heidelberg.
Sperry JS, Holbrook NM, Zimmermann MH, Tyree MT (1987) Spring filling of xylem vessels in wild grapevine. Plant Physiol 83:414–417.
Sperry J, Hacke U, Oren R, Comstock J (2002) Water deficits and hydraulic limits to leaf water supply. Plant Cell Environ 25:251–263.
Stiller V, Sperry JS, Lafitte R (2005) Embolized conduits of rice (*Oryza sativa*, Poaceae) refill despite negative xylem pressure. Am J Bot 92: 1970–1974.
Stroock AD, Pagay VV, Zwieniecki MA, Michele Holbrook N (2014) The physicochemical hydrodynamics of vascular plants. Annu Rev Fluid Mech 46:615–642.
Taiz L (2006) Plant physiology, 4th ed. Sinauer, Sunderland, MA.
Temperley H, Trevena D (1994) Metastability of the liquid-vapor transition and related effects. J Statist Phys 77:501–508.
Tötzke C, Miranda T, Konrad W, Gout J, Kardjilov N, Dawson M, Manke I, Roth-Nebelsick A (2013) Visualization of embolism formation in the xylem of liana stems using neutron radiography. Ann Bot (Lond) 111: 723–730.
Trifilò P, Raimondo F, Lo Gullo MA, Barbera PM, Salleo S, Nardini A (2014) Relax and refill: xylem rehydration prior to hydraulic measurements favours embolism repair in stems and generates artificially low PLC values. Plant Cell Environ 37:2491–2499.
Tyree MT, Sperry JS (1989) Vulnerability of xylem to cavitation and embolism. Annu Rev Plant Biol 40:19–36.
Tyree MT, Zimmermann MH (2002) Hydraulic architecture of whole plants and plant performance. In: Xylem structure and the ascent of sap. Springer, pp 175–214.
Tyree MT, Salleo S, Nardini A, Gullo MAL, Mosca R (1999) Refilling of embolized vessels in young stems of laurel. Do we need a new paradigm? Plant Physiol 120:11–22.
Venturas MD, Sperry JS, Hacke UG (2017) Plant xylem hydraulics: What we understand, current research, and future challenges. J Integr Plant Biol 59:356–389.
Vergeynst LL, Dierick M, Bogaerts JA, Cnudde V, Steppe K (2014) Cavitation: a blessing in disguise? New method to establish vulnerability curves and assess hydraulic capacitance of woody tissues. Tree Physiol 35:400–409.
Vesala T, Hölttä T, Perämäki M, Nikinmaa E (2003) Refilling of a hydraulically isolated embolized xylem vessel: model calculations. Ann Bot (Lond) 91:419–428.
Vogt UK (2001) Hydraulic vulnerability, vessel refilling, and seasonal courses of stem water potential of *Sorbus aucuparia* L. and *Sambucus nigra* L. J Exp Bot 52:1527–1536.
Wang R, Zhang L, Zhang S, Cai J, Tyree MT (2014) Water relations of *Robinia pseudoacacia* L.: do vessels cavitate and refill diurnally or are R-shaped curves invalid in *Robinia*? Plant Cell Environ 37: 2667–2678.
Wei C, Tyree MT, Steudle E (1999) Direct measurement of xylem pressure in leaves of intact maize plants. a test of the cohesion-tension theory taking hydraulic architecture into consideration. Plant Physiol 121: 1191–1205.
Wheeler JK, Huggett BA, Tofte AN, Rockwell FE, Holbrook NM (2013) Cutting xylem under tension or supersaturated with gas can generate PLC and the appearance of rapid recovery from embolism. Plant Cell Environ 36:1938–1949.